HHS Public Access

Author manuscript

Traffic. Author manuscript; available in PMC 2015 October 07.

Published in final edited form as:

Traffic. 2011 October ; 12(10): 1417–1431. doi:10.1111/j.1600-0854.2011.01243.x.

Derlin-Dependent Retrograde Transport from Endosomes to the Golgi Apparatus

Hope Dang[1], **Tove I. Klokk**[2,3], **Basil Schaheen**[1,4], **Brooke M. McLaughlin**[1], **Anthony J. Thomas**[1], **Tyler A. Durns**[1], **Benjamin G. Bitler**[5], **Kirsten Sandvig**[2,3,6], and **Hanna Fares**[1,*]

[1]Department of Molecular and Cellular Biology, Life Sciences South Room 531, University of Arizona, Tucson, AZ 85721

[2]Department of Biochemistry, Institute for Cancer Research, The Norwegian Radium Hospital, Oslo University Hospital, 0310 Oslo, Norway

[3]Centre for Cancer Biomedicine, Faculty of Medicine, University of Oslo, 0310 Oslo, Norway

[4]Jefferson Medical College, Philadelphia, PA 19107

[5]Cancer Biology Program, University of Arizona, Tucson, AZ 85721

[6]Department of Molecular Biosciences, Faculty of Mathematics and Natural Sciences, University of Oslo, 0316 Oslo, Norway

Abstract

Cells have to maintain stable plasma membrane protein and lipid compositions under normal conditions and to remodel their plasma membranes in response to stimuli. This maintenance and remodeling require that integral membrane proteins at the plasma membrane that become misfolded, due to the relatively harsher extracellular milieu or carbohydrate and amino acid sequence changes, are degraded. We had previously shown that Derlin proteins, required for quality control mechanisms in the Endoplasmic Reticulum, also localize to endosomes and function in the degradation of misfolded integral membrane proteins at the plasma membrane. In this study, we show that Derlin proteins physically associate with Sorting Nexins that function in retrograde membrane transport from endosomes to the Golgi apparatus. Using genetic studies in *Caenorhabditis elegans* and ricin pulse-chase analyses in murine RAW264.7 macrophages, we show that the Derlin-Sorting Nexin interaction is physiologically relevant. Our studies suggest that at least some integral membrane proteins that are misfolded at the plasma membrane are retrogradely transported to the Golgi apparatus and ultimately to the Endoplasmic Reticulum for degradation via resident quality control mechanisms.

Keywords

Derlin; Retromer; Sorting Nexin; *C. elegans*; Ricin; ERAD; Endocytosis; Misfolded Proteins

*Corresponding author: Hanna Fares, fares@email.arizona.edu.

COMPETING FINANCIAL INTERESTS

The authors declare that they have no competing financial interests.

INTRODUCTION

Systems that are used to identify misfolded proteins and to target them for degradation are being elucidated in different cellular compartments, including the cytoplasm, the nucleus, and the Endoplasmic Reticulum (ER) (1-3). These systems include modules that recognize proteins as misfolded, tag them with ubiquitin, and target them for degradation by the proteasome.

Proteins destined for the secretory pathway, including integral membrane proteins, are imported into the ER through the SEC61 channel complex (4, 5). In the ER, proteins that are recognized as misfolded are retrotranslocated to the cytoplasm for degradation by the proteasome, a process referred to as ER-Associated Degradation (ERAD) (6, 7). While there is substantial evidence for a direct role of the SEC61 channel, studies have implicated another family of proteins, Derlins, in this retrotranslocation (8-14). Derlin proteins have four predicted membrane-spanning domains and are conserved in all eukaryotes. There are two members in *Saccharomyces cerevisiae*, Der1p and Dfm1p, two in *Caenorhabditis elegans*, CUP-2 and R151.6, and three in humans, Derlin-1, Derlin-2, and Derlin-3.

There is increasing evidence for quality control mechanisms that monitor the folding of integral membrane proteins at the plasma membrane and/or endosomes. In mammalian cells, several receptors that are misfolded at the plasma membrane are degraded more rapidly than their properly folded counterparts; these include unliganded Major Histocompatibility Complex Type I, Low Density Lipoprotein Receptor misfolded extracellular domain, Cystic Fibrosis Transmembrane Conductance Regulator (CFTR) cytoplasmic domain mutants, α2A-Adrenergic Receptor transmembrane domain mutant, Dopamine D4.4 Receptor transmembrane domain mutant, and Vasopressin V2 Receptor cytoplasmic domain mutant (15-20). Recent studies identified chaperones and ubiquitin ligases that function in the degradation of misfolded CFTR, Dopamine D4.4 Receptor, and Vasopressin V2 Receptor at the plasma membrane (15, 21).

Our previous studies indicated that Derlins also function in quality control mechanisms of protein folding at the plasma membrane/endosomes (18). We showed that *C. elegans* and mammalian Derlins localize to endosomes, in addition to the ER. In *C. elegans*, we showed that null mutations in *cup-2* (encodes one of the Derlins) results in the accumulation of MCA-3 (a Membrane Calcium ATPase) at the plasma membrane; this accumulation is independent of the ERAD functions of CUP-2 protein. We showed that murine RAW264.7 macrophages that have reduced levels of Derlin-1 similarly also accumulate several integral membrane proteins at the plasma membrane. Furthermore, we showed that misfolding the extracellular domain of the Low Density Lipoprotein Receptor at the plasma membrane results in a Derlin-1-dependent increased rate of its degradation.

Sorting Nexins (SNXs) are a diverse group of cytoplasmic and membrane-associated proteins that are defined by the presence of an SNX phox homology (PX) domain, a subgroup of the PX domain superfamily (22, 23). Snx1 and Snx2, like other mammalian orthologues of the yeast retromer complex, are required for the retrograde transport of proteins from endosomes to the Golgi apparatus (24-27). Although mammalian Snx2

colocalizes with Snx1, genetic studies in mice using *Snx1* and *Snx2* knockouts have shown that these two genes have largely, but not exclusively, redundant functions (28). *C. elegans* SNX-1 is ~50% identical to mammalian Snx1 and Snx2. Indeed, *C. elegans* SNX-1 also functions in the retrograde transport of proteins from endosomes to the Golgi apparatus (29).

In this study, we show that *C. elegans* and mammalian Derlins physically associate with Sorting Nexins. We provide data in both systems that this interaction is physiologically relevant. Our results are consistent with a model whereby at least some integral membrane proteins that become misfolded at the plasma membrane undergo Derlin/Sorting Nexin-dependent retrograde membrane transport to the Golgi apparatus and eventually to the ER for degradation via ERAD.

RESULTS

C. elegans *CUP-2 and SNX-1 Physically Associate*

Previous genome-wide conventional yeast two-hybrid studies suggested an interaction between *C. elegans* CUP-2 and Sorting Nexin-1 (SNX-1) (30). We first confirmed this interaction using full-length proteins: CUP-2 but not R151.6, the second *C. elegans* Derlin, interacts with SNX-1 by conventional yeast two-hybrid assays (Figure 1A). We then used the split-ubiquitin yeast two-hybrid system to confirm the interaction of *C. elegans* CUP-2 and SNX-1. This variant yeast two-hybrid system can assay full-length integral membrane proteins (31). The advantages of this system are that full-length integral membrane proteins are assayed and the fusion proteins are not artificially targeted to the nucleus such that interactions are assayed in cytoplasmic compartments, albeit in yeast cells. The CUP-2-Cub and R151.6-Cub fusion proteins showed an interaction with the positive controls, the plasma membrane-localized Fur4-NubI and the ER-localized Ost1-NubI, indicating that the Cub-LexA-VP16 domains are in the cytoplasm (the topology of the proteins are correct) and that these overexpressed fusion proteins localize to the ER and/or to the plasma membrane of yeast cells (Figure 1B). The CUP-2-Cub and R151.6-Cub fusion proteins do not show non-specific interactions with the negative controls Fur4-NubG or Ost1-NubG (Figure 1B). CUP-2-Cub interacts with NubG fusions of CUP-2, R151.6, and SNX-1, while R151.6-Cub interacts with NubG fusions of CUP-2 and R151.6, but not with the NubG fusion of SNX-1 (Figure 1B). These yeast two hybrid studies suggest that CUP-2 and R151.6 homo-dimerize and hetero-dimerize and that CUP-2, but not R151.6, interacts with SNX-1.

We carried out immunoprecipitation studies to confirm the CUP-2 interaction with SNX-1. Transgenic *C. elegans* strains expressing a functional GFP::SNX-1 fusion protein had already been described (29). We made transgenic *C. elegans* strains that express CUP-2::3xFLAG under the control of the *cup-2* promoter; this CUP-2::3xFLAG is functional because it rescues the *cup-2(ar506)* null mutant's ERAD defect (indirectly assayed since defective ERAD activates the Unfolded Protein Response measured by the activation of an *hsp-4::GFP* reporter) and the coelomocyte endocytosis defect (visualized as a defect in the uptake by macrophage-like cells called coelomocytes of GFP secreted by muscle cells into the body cavity) (Supplementary Figure S1) (18). We immunoprecipitated (IP'd) CUP-2::3xFLAG proteins from membrane preparations of worm lysates of strains co-expressing GFP::SNX-1 and CUP-2::3xFLAG proteins, using as controls lysates from

strains expressing each fusion protein individually (Figure 1C). Consistent with the yeast two-hybrid results, we detected GFP::SNX-1 in IPs of CUP-2::3xFLAG, indicating that CUP-2 and SNX-1 physically associate (Figure 1C).

We confirmed the in vivo association o f CUP-2 and of SNX-1 using co-localization studies. We had previously shown that *C. elegans* and mouse Derlins localize to endosomes, in addition to the ER (18). *C. elegans* SNX-1 had previously been localized to early endosomes in several tissues (29). We confirmed this SNX-1 localization in coelomocytes: *C. elegans* SNX-1 shows complete co-localization with the early endosomal marker RAB-5 in compartments close to the plasma membrane of coelomocytes (Figure 1D). Consistent with these results, while the majority of CUP-2::GFP localized to a perinuclear ER compartment (asterisks in Figure 1E), we consistently detected CUP-2 that co-localized with SNX-1 around peripheral compartments close to the plasma membrane (arrows in Figure 1E). Given the complete co-localization of SNX-1 and of RAB-5, these results indicate that some CUP-2 associate with SNX-1 at endosomal membranes.

Having established that *C. elegans* CUP-2 interacts and co-localizes on endosomes with SNX-1, we analyzed *snx-1* null mutant worms to determine the functional significance of this interaction.

snx-1 Mutant Phenocopies Plasma Membrane/Endosomal Defects of cup-2 *Mutant*

We had previously shown that the *cup-2(ar506)* null mutant shows several defects in coelomocytes: an ERAD defect (observed as an activation of the Unfolded Protein Response), a mild endocytosis defect, accumulation of MCA-3 (a Membrane Calcium ATPase) at the surfaces (plasma membrane and early endosomes) of cells, and increased plasma membrane/endosome association of Clathrin Heavy Chain (18). Using the *snx-1(tm847)* null allele, we first ascertained that, lack of SNX-1 does not cause a detectable increase in UPR (Figure 2A, B) (29). Therefore as predicted, SNX-1 does not function in ERAD.

snx-1(tm847); p*myo-3::ssGFP* worms show a clear increase in GFP levels in the body cavity, indicating a defect in endocytosis by coelomocytes (Figure 2C, D). This endocytosis defect is not severe since the sizes of the GFP-filled compartments are not significantly smaller than those in wild type worms (Figure 2C, D). Similar to the *cup-2* null mutant, the *snx-1(tm847)* endocytosis defect is temperature sensitive being more severe at elevated temperatures (Supplementary Figure S2) (18). Indeed, and unlike any other *cup* null mutant, neither *cup-2* nor *snx-1* null mutant has a coelomocyte endocytosis defect at lower temperatures (Supplementary Figure S2) (18, 32).

cup-2(ar506) null mutant accumulates MCA-3 at the plasma membrane and/or endosomes of coelomocytes; this accumulation is not a consequence of the endocytosis defect (18). By quantitative microscopy, *snx-1(tm847)* null mutant shows an increase in MCA-3 levels at the surface of coelomocytes (Figure 2E, H). The increase in the plasma membrane levels of MCA-3 in *cup-2* and in *snx-1* mutants is equivalent (P 0.8) (Figure 2G). These microscopy determinations were confirmed using Western blot analysis of immunoprecipitated (IP'd) GFP::MCA-3 that showed an increase in total GFP::MCA-3 levels in the coelomocytes of

cup-2 and *snx-1* mutants (Figure 2F, G). From three independent IP experiments, GFP::MCA-3 in the coelomocytes of *cup-2* mutant worms were 1.73 +/- 0.05 times the levels in wild type and GFP::MCA-3 in the coelomocytes of *snx-1* mutant worms were 1.87 +/- 0.32 times the levels in wild type, in agreement with the microscopy measurements. In contrast, and similar to *cup-2* mutant, *snx-1* mutant does not show differences relative to wild type in the levels of integral membrane proteins that localize to the Golgi apparatus (Mannosidase II) or to lysosomes (CUP-5) (Figure 2E, H) (18). Consistent with the results of the endocytosis assay, and like *cup-2* mutant, *snx-1(tm847)* shows an accumulation of Clathrin Heavy Chain at the surface of coelomocytes (Figure 2E, H).

These results indicate that the *snx-1* null mutant exhibits the same plasma membrane/surface defects as the *cup-2* null mutant. In wild type coelomocytes, MCA-3 is recycled back to the plasma membrane following its endocytosis (18). To determine the reason for the MCA-3 accumulation in *cup-2* and *snx-1* mutant, we determined the trafficking itinerary of MCA-3 in these mutant backgrounds.

MCA-3 is Recycled to the Plasma Membrane in the Absence of CUP-2 or SNX-1

We used mutations that block recycling or lysosomal degradation to determine the fate of MCA-3 in *cup-2* and *snx-1*null mutants (see Figure 7). *rme-1(b1045)* null mutant blocks the exit of recycling proteins from recycling compartments of most tissues leading to an expansion of these recycling endosomes (33). We had previously shown that in *rme-1(b1045)*, MCA-3 localizes to these expanded recycling endosomes in coelomocytes (Figure 3A) (18). *cup-5(ar465)* mutant blocks lysosomal degradation resulting in the accumulation of proteins in dramatically expanded compartments (34, 35). We had previously shown that in *cup-5(ar465)*, MCA-3 does not appear/weakly localizes to enlarged vacuoles in coelomocytes (Figure 3A) (18). Thus, under normal growth conditions, most of MCA-3 in coelomocytes is recycled back t o t he plasma membrane following its endocytosis. That is, if a portion of this MCA-3 in wild type *C. elegans* is misfolded, most of this misfolded MCA-3 is recycled to the plasma membrane instead of transported to lysosomes for degradation. Similarly, MCA-3 primarily accumulates in expanded recycling endosomes of *rme-1* null mutant and weakly in enlarged vacuoles of *cup-5* mutant in the absence of CUP-2 or SNX-1 (Figure 3A). Thus, in the absence of CUP-2 or SNX-1, most of MCA-3 is still recycled to the plasma membrane. Consistent with the increased MCA-3 levels in the single *cup-2* and *snx-1* null mutants, *cup-2; rme-1* and *snx-1; rme-1* double mutants show increased GFP::MCA-3 levels on expanded recycling endosomes relative to *rme-1* single mutant (Figure 3B).

Some Retromer Mutants Phenocopy Plasma Membrane/Endosomal Defects of cup-2 *and* snx-1 *Mutants*

We wanted to determine whether SNX-1 functioned with Derlin-1 in the context of its roles in retromer. The retromer complex mediates the retrograde transport of vesicles from endosomes to the Golgi apparatus and is composed of two complexes: an Snx1/2-Snx5/6 dimer that functions in conjunction with a Vps26-Vps29-Vps35 trimer (36, 37). *snx-6(tm3790)*, *vps-29(tm1320)*, and *vps-35(hu68)* are deletion, presumed null, alleles of these retromer components . We used these to determine whether loss of retromer function

results in endocytosis and/or MCA-3 accumulation defects, similar to *cup-2* and *snx-1* null mutants.

We first checked the coelomocyte endocytosis phenotypes of retromer mutants using the p*myo-3::ssGFP* assay. *snx-6* mutant showed a clear increase in sizes of GFP-filled compartments in coelomocytes at 25° while *vps-29* mutant showed a clear increase in sizes of GFP-filled compartments in coelomocytes at 15º. This indicates that both SNX-6 and VPS-29 function in coelomocytes (Supplementary Figure S3A). However, only *vps-35* mutant showed clear reduced uptake of GFP by coelomocytes characterized by accumulation of GFP in the body cavity and reduced sizes of GFP-filled compartments (Supplementary Figure S3A). Furthermore, and similar to both *cup-2* and *snx-1* null mutants, the *vps-35* mutant endocytosis defect by coelomocytes was temperature sensitive such that endocytosis was normal at 15° and became more severely defective as the temperature was elevated: at 20°, GFP accumulated in the body cavity with a minor reduction in sizes of GFP-filled compartments in coelomocytes and at 25°, GFP accumulated in the body cavity with a larger reduction in sizes of GFP-filled compartments in coelomocytes (Supplementary Figure S3A).

We then assayed levels of GFP::MCA-3 in the retromer mutants. We used 20° and 25°, the temperatures at which *vps-35* mutant shows a defect in coelomocyte endocytosis. Consistent with the p*myo-3::ssGFP* assay, and similar to *cup-2* and *snx-1* null mutants, *vps-35* mutant showed significantly elevated levels of MCA-3 at the surfaces of coelomocytes at both temperatures (Supplementary Figure S3B). Furthermore, while *snx-6* mutant did not show a noticeable uptake defect by the p*myo-3::ssGFP* assay (which is relatively weak in *cup-2*, *snx-1*, and *vps-35* mutants), this mutant also showed significantly elevated levels of MCA-3 at the surfaces of coelomocytes at both temperatures (Supplementary Figure S3B). *vps-29* mutant did not show an effect on MCA-3 levels at either temperature. Thus, *cup-2*, *snx-1*, *snx-6*, and *vps-35* mutants have similar effects on MCA-3 levels at the surfaces of coelomocytes.

These studies suggested a model where in wild type worms, MCA-3 (and other proteins) at the plasma membrane become misfolded and associate with CUP-2 in endosomes (see Figure 7). CUP-2 directly or indirectly interacts with SNX-1 and at least some retromer proteins (SNX-6 and VPS-35) resulting in the retrograde transport of this complex to the Golgi apparatus and ultimately to the ER for degradation via ERAD. In the absence of CUP-2 or SNX-1, and likely SNX-6 or VPS-35, misfolded MCA-3 is not degraded by this pathway and instead recycles to the plasma membrane leading to an increase in MCA-3 levels at the surfaces of cells. The significance of these studies was that they were done in vivo, that is on cells within t h e i r normal niche in organisms. Furthermore, these studies utilized homogenous populations that had complete knockouts of gene functions. However, the limitation of these in vivo studies is that they do not allow for biochemical assays that measure rates of some membrane transport steps. We therefore initiated complimentary studies in mammalian tissue-culture cells to directly measure rates of retrograde transport from endosomes to the Golgi apparatus. We chose murine macrophages as a model because of their similarity to *C. elegans* coelomocytes, thus allowing easier comparisons between the two systems.

Mammalian Derlins and Sorting Nexins Physically Associate

We first confirmed that, similar to *C. elegans*, mouse Derlins physically associate with Sorting Nexins . We IP'd mouse Derlin-1-GFP or GFP-TRPML1 (a lysosomal integral membrane protein) from stable RAW264.7 clones that express these fusion proteins (18, 38). We then used Mass Spectrometry to identify proteins in each mixture; we considered candidate Derlin-1 mouse interactors proteins that co-IP'd with Derlin-1-GFP but not GFPTRPML1. These candidate Derlin-1-GFP interactors included various proteins of the ERAD machinery, including some (E2 Ubiquitin Conjugating Enzymes, Superoxide Dismutase, Disulfide Isomerase) that had previously been shown to interact with Derlin-1 (Supplementary Table 1) (39-42). In addition, we identified Sorting Nexin 2 (Snx2) as a candidate Derlin-1 interactor (Supplementary Table 1) (43).

We confirmed the association of Derlin-1 with Sorting Nexins by IP after overexpression of epitope-tagged proteins. HeLa cells were transfected with a GFP-expressing plasmid (pEGFP-C3) or with a plasmid that expresses mouse Derlin-1-GFP. Cells were co-transfected with plasmids that express 3xFLAG epitope fused to mouse Snx1, Snx2, or Snx4. Snx1, Snx2, and Snx4 IP'd specifically with Derlin-1-GFP, indicating that these Sorting Nexins physically associate with Derlin-1 (Figure 4A).

We also confirmed that endogenous Derlin-1 and Derlin-2 associate with Sorting Nexins. We performed IPs on lysates of murine RAW264.7 macrophage using antibodies that are specific to mouse Derlin-1, Derlin-2, or Destrin (an actin binding protein) as a control. We probed the Western blots of these IPs with antibodies against relevant proteins, though we could not use antibodies against Snx1 because of the presence of cross-reacting IgG heavy chain molecules in the IPs that have a similar size to Snx1.

In Derlin-1 IPs, we detected Derlin-2, Snx2, and Snx4 (Figure 4B). Similarly, in Derlin-2 IPs, we detected Derlin-1, Snx2, and Snx4 (Figure 4B). Our negative controls clearly showed that we did not detect any Sorting Nexins in IPs of Destrin or when no antibodies were included in the IPs (Figure 4B) (44). The IP results indicate that mouse Derlin-1 and Derlin-2 physically associate with Snx1, Snx2, and Snx4.

We used the split-ubiquitin yeast two-hybrid system as another test of the Sorting Nexin-Derlin interaction. Mouse Derlin-1-Cub and Derlin-2-Cub fusion proteins showed an interaction with the plasma membrane-localized Fur4-NubI and the ER-localized Ost1-NubI, indicating that the Cub domains are in the cytoplasm and that the overexpressed fusion proteins localize to the ER and/or to the plasma membrane of yeast cells (Figure 4C). However, while the Derlin-2-Cub protein did not show non-specific interactions with the negative controls Fur4-NubG or Ost1-NubG, the Derlin-1-Cub protein interacted with Ost1-NubG but not with Fur4-NubG (Figure 4C). The interaction of Derlin-1-Cub with Ost1-NubG may indicate that the Derlin-1-Cub interacts nonspecifically with other proteins or that this interaction may be between the Derlin-1-Cub and a misfolded pool of Ost1-NubG in the ER. We favor the latter possibility because Derlin-1-Cub did not interact with Snx4-NubG. Both Derlin-1-Cub and Derlin-2-Cub interacted with NubG fusions of Derlin-1 and Derlin-2, consistent with previous studies that showed that these proteins homo- and heterodimerize (Figure 4C) (45). Furthermore, both Derlin-1-Cub and Derlin-2-Cub

interacted with NubG fusions of Snx1 and Snx2, but not Snx4. Therefore, by this assay, Derlin-1 and Derlin-2 associate with Snx1 and Snx2. Note that we detected an interaction between Derlins and Snx4 by IP but not by this yeast two-hybrid assay. Thus, both the IP and the yeast two-hybrid assays consistently show that Derlin-1 and/or Derlin-2 associate with Snx2 and likely with Snx1.

We had previously shown that Derlin-1 and Derlin-2 both localize to endosomes (in addition to the ER) and that a separate pool of Derlin-1 and Derlin-2 cofractionates with Snx1 and Snx2 (18). We used immunofluorescence of fixed cells to confirm that Derlins and Sorting Nexins co-localize in vivo. Of the Sorting Nexins, only anti-Snx2 antibodies worked on RAW264.7 cells using different fixation protocols. Similar to CUP-2 and SNX-1, and consistent with the physical association studies, we saw a clear co-localization between Derlin-1 and Snx2 and between Derlin-2 and Snx2 on peripheral compartments (Figure 4C).

Association of Mammalian Derlins with Retromer Proteins

Given the association of mouse Derlin-1 and Derlin-2 with Snx2 and the phenotypes of the retromer *C. elegans* mutants, we determined whether mammalian Derlins associate with other proteins of the retromer complex. We tested the association of human Derlin-1, Derlin-2, and Derlin-3 with Retromer proteins by IP after overexpression of epitope-tagged proteins. HeLa cells were transfected with a GFP-expressing plasmid (pEGFP-C3) or with plasmids that expresses human Derlin1/2/3-GFP. Cells were cotransfected with plasmids that express 3xFLAG epitope fused to human retromer proteins and the Derlin-GFP was IP'd.

All three human Derlins showed similar interaction patterns, with Derlin-2 showing the strongest interactions with retromer proteins. Of the Sorting Nexins, human Derlins associate strongly with Snx2, weakly with Snx1 and Snx6, and do not associate with Snx5 (Supplementary Figure S4). The weak interaction with Snx1 and Snx6 could be indirect through Snx2 or may be a consequence of the overexpression of the proteins. None of the human Derlins associate with Vps26, Vps29, or Vps35, although the 3XFLAG-Vps35 plasmid did no t give significant overexpression to ascertain lack of an indirect interaction with Derlins (Supplementary Figure S5). Taken together with the *C. elegans* retromer mutant analysis, these results suggest that Derlins associate directly with Snx2, thus recruiting other members of the retromer complex, at least Snx6 and Vps35, to effect their retrograde transport to the Golgi apparatus. We next directly assayed Derlin-dependent retrograde transport.

Misfolding of Plasma Membrane Proteins Increases Ricin Retrograde Transport

Ricin is a potent protein cytotoxin that is derived from the castor bean *Ricinus communis*. Ricin is a heterodimer composed of a catalytically active “A” chain joined by a disulfide bond to a galactose specific “B” chain. Thericin B chain binds to glycosylated extracellular domains of integral membrane proteins at the plasma membrane. Ricin is internalized by several mechanisms at the cell surface and is transported to early endosomes (46). From early endosomes, a small portion of ricin is retrogradely transported to the Golgi apparatus and then to the ER where the ricin A chain is exported to the cytoplasm via ERAD and

effects its toxicity (47, 48). Importantly, the retrograde transport of ricin from endosomes to the Golgi apparatus requires Retromer and Sorting Nexins, including Snx2 (49, 50).

The small amounts of ricin that are retrogradely transported to the Golgi apparatus and the Snx2 requirement suggested that ricin partly binds to misfolded integral membrane proteins at the plasma membrane, some of which associate with Derlins in early endosomes leading to their retrograde transport to the Golgi apparatus via the Derlin-Snx2 interaction. There are two predictions from such a system. First, increasing misfolding at the plasma membrane should lead to more ricin retrograde transport. Second, ricin retrograde transport should be dependent on Derlin functions.

Exposing cells to a high salt, low pH buffer (MFB-1) for 5 minutes at 4° leads to misfolding of proteins at the plasma membrane and their faster degradation in a Derlin-dependent manner (18). Indeed, MFB-1 treatment leads to increased ricin cytotoxicity of murine RAW 264.7 macrophages; PBS pre-treatment or MFB-1 pre-treatment before ricin exposure results in 100+/-7% viability (PBS) versus 100+/-6% viability (MFB-1) at 0 ng/ml ricin (*P* 0.99), 95+/-3% viability (PBS) versus 87+/-3% viability (MFB-1) at 1 ng/ml ricin (*P* 0.02), and 21+/-2% viability (PBS) versus 13+/-1% viability (MFB-1) at 100 ng/ml ricin (*P* 0.003) (Figure 5A). We note that the small increase in ricin toxicity after MFB-1 treatment was expected because we only treated cells with MFB-1 once such that, over the 24 hour incubation of cells with ricin, there was a single initial increase in the number of misfolded proteins that would bind ricin after which those misfolded proteins are degraded and the MFB-1-treated cells would have the same levels of misfolded proteins as PBS-treated cells. We therefore directly assayed whether MFB-1 treatment results in increased ricin retrograde transport to the Golgi apparatus.

RS1, a ricin variant containing a modified ricin A-chain with a tyrosine sulfation site reconstituted with ricin B chain, allows for measurements of rates of retrograde transport from endosomes to the Golgi apparatus (where the tyrosine is sulfated by resident enzymes) (51). In pulse-chase experiments, RS1 showed a dramatic ~1.6x increase in sulfation in MFB-1-treated relative to PBS-treated RAW264.7 macrophages (Figure 5B, C). This ~1.6x is an underestimate because there was a slight decrease (~20 %) of endocytosed RS1 in MFB-1-treated relative to PBS-treated cells (Figure 5B). Finally, there was only a minor difference in total sulfation levels between MFB-1-treated and PBS-treated cells (~10 %), indicating that levels and activities of the tyrosylprotein sulfotransferases (TPSTs) in the Golgi apparatus were not significantly affected by the MFB-1 treatment (Figure 5C). Thus, misfolding plasma membrane integral membrane proteins results in an increase in ricin retrograde transport from endosomes to the Golgi apparatus. We therefore determined whether this retrograde transport is dependent on Derlin-1.

Ricin Retrograde Transport Requires Derlin-1

We had previously made stable RAW264.7 clones that express a Derlin-1 shRNA construct and that showed ~8.2% of the Derlin-1 protein levels compared to RAW264.7 (18). To ensure that effects we observe are due to compromised Derlin-1 functions, we assayed in parallel stable RAW264.7 clones that overexpress a Derlin-1-GFP dominant-negative fusion protein (18, 52). Indeed, both stable clones showed similar ~40% reductions in total protein

synthesis, likely due to the activation of the Unfolded Protein Response due to defects in ERAD (Figure 6A) (53).

We first assayed whether these Derlin-1-compromised clones show resistance to ricin toxicity after prolonged exposure to this toxin. Indeed, Derlin-1-GFP and Derlin-1 shRNA clones showed almost identical increased resistance to ricin cytotoxicity, with a 3.5- and 4-fold protection, respectively, relative to RAW264.7 (Figure 6B). This increased resistance is unlikely to be due to an ERAD defect in the Derlin-1-compromised clones since previous results using similar Derlin-GFP dominant negative constructs showed that the ERAD-mediated retrotranslocation of ricin A to the cytoplasm is independent of Derlin-1 or Derlin-2 functions but is dependent on Sec61 channel (54). This increased resistance to ricin cytotoxicity was therefore likely due to a Derlin requirement at an earlier transport step.

We assayed the rates of ricin endosome to Golgi apparatus transport using RS1. In pulse-chase experiments, Derlin-1-compromised clones showed a dramatic decrease in sulfation of RS1, to ~10% of RAW264.7 macrophages (Figure 6C, D). Consistent with the reduction in total protein synthesis (including TPSTs), Derlin-1-compromised clones showed total sulfation levels that were ~50% of RAW264.7 cells (Figure 6A, D). Furthermore, and consistent with the reduced endocytosis rate of *C. elegans cup-2* mutant coelomocytes, Derlin-1-compromised clones' endocytosis of RS1 was ~85% of RS1 uptake in RAW264.7 cells (Figure 6C) (18). We note that the endocytosis defects in *C. elegans cup-2* mutants or RAW264.7 Derlin-1 shRNA clones are relatively mild (*cup-2* is the weakest identified *cup* mutant) and that neither system showed significant defects in other membrane transport steps, for example transport to lysosomes (18, 32). When we normalize RS1 sulfation values taking into account the decrease in total sulfation and endocytosis of RS1, Derlin-1-compromised clones still show a significant decrease in sulfation of RS1 to ~25% of RAW264.7 macrophages. Thus, Derlin-1 is required for the efficient retrograde transport of ricin from endosomes to the Golgi apparatus.

DISCUSSION

In this study, we show that Derlins and Sorting Nexins show conserved physical association and co-localization to endosomes. We also show that *C. elegans snx-1*, *snx-6*, and *vps-35* null mutants accumulate MCA-3 at the surfaces of coelomocytes. This phenotype is identical to *cup-2* null mutant and is not seen in other *cup* mutants that disrupt membrane trafficking in coelomocytes (32). We think, but cannot test using this in vivo system, that under normal growth conditions, some MCA-3 becomes misfolded such that the degradation of this misfolded MCA-3 requires CUP-2, SNX-1, SNX-6, VPS-35, and potentially other proteins. In the absence of CUP-2, SNX-1, SNX-6, or VPS-35, this misfolded MCA-3 is not degraded and recycles to the plasma membrane leading to its increased levels at the plasma membrane/endosomes . MCA-3 accumulation results in Clathrin Heavy Chain recruitment and a mild defect in endocytosis by coelomocytes. This is consistent with the temperature-sensitivity of the *cup-2*, *snx-1*, and *vps-35* null endocytosis defects since less MCA-3 is predicted to misfold in the animals grown at lower than at higher temperatures. We do not know why the *snx-6* mutant did not show a similar uptake defect; we suspect that this is due to the sensitivity of the GFP uptake assay since *cup-2*, *snx-1*, and *vps-35* mutants only show

a mild defect relative to other *cup* mutants by this assay. Alternatively, *snx-6* may have other functions in the endocytic pathway that suppress the uptake defect; indeed, unlike *cup-2*, *snx-1*, and *vps-35* mutants, the *snx-6* mutant shows increased sized of endosomes/lysosomes relative to wild type at 25°.

Because of the Derlin-SNX association, we used the mammalian system to probe retrograde transport. We had previously shown that the degradation of misfolded integral membrane proteins requires Derlin-1. In the absence of biochemical assays for integral membrane proteins in cells, we used ricin transport as an indirect measure of the retrograde pathway. Indeed, we showed that ricin retrograde transport is significantly increased after misfolding plasma membrane proteins, indicating that ricin binds to misfolded receptors at the plasma membrane and that some of these misfolded receptors that bind ricin are retrogradely transported from endosomes to the Golgi apparatus. Under normal conditions only a small fraction of endocytosed ricin reaches the Golgi apparatus, which may partly be due to the fact that only a small fraction of integral membrane proteins are misfolded under normal growth conditions. Our data also show that the retrograde transport of ricin requires Derlin-1, thus implicating endosomal Derlin-1 protein in this pathway.

Our studies show the presence of a novel pathway for the degradation of misfolded proteins at the plasma membrane. Our model is that at least some integral membrane proteins that become misfolded associate with Derlins in endosomes following their internalization (Figure 7). This association results in the retrograde transport of the Derlin-Misfolded Protein complex by SNX/Retromer (at least some components) to the Golgi apparatus, and ultimately to the ER where the misfolded proteins are degraded via ERAD. This pathway from endosomes to ERAD is, for example, one of the steps used for the cross-presentation of soluble antigens by Major Histocompatibility Complex Type I in dendritic cells and involves the transport of soluble antigens to the ER following their endocytosis (55). Also, several plant and bacterial toxins, including ricin, traffic to the ER following their endocytosis and use ERAD to reach the cytoplasm (56). In the absence of Derlins or SNX/Retromer, some misfolded proteins recycle to the plasma membrane leading to their accumulation (Figure 7).

An alternative to the proposed retrograde pathway is that misfolded proteins at the plasma membrane could be transported to lysosomes for degradation (Figure 7). For example, while wild type CFTR recycles to the plasma membrane following its endocytosis, misfolded CFTR is ubiquitinated and targeted for lysosomal degradation (19). We do not know whether Derlins are required for lysosomal targeting of misfolded proteins like CFTR. Finally, our studies focused on Derlin-1. We do not know whether Derlin-2 and Derlin-3 functions in any aspects of these surface quality control mechanisms. Derlin-2 is likely to function alone or as a hetero-dimer with Derlin-1 since Derlin-2 also interacts with Snx2 on endosomes.

We propose that this Derlin/SNX-mediated retrograde transport quality control pathway is essential for the degradation of proteins that normally recycle efficiently to the plasma membrane, for example MCA-3 in *C. elegans* coelomocytes. Such proteins that either are poor ubiquitination substrates when misfolded (for example due to misfolding of

extracellular domains or that do not have accessible lysines in their cytoplasmic domains for ubiquitination) or that have strong recycling determinants would require alternative routes for their degradation. Indeed, since most integral membrane proteins at the plasma membrane have long half-lives and follow a recycling route after their internalization, this pathway may also be required for the remodeling of membranes during normal responses to stimuli or during development (57, 58). This pathway may also contribute to or prevent the development of diseases that require considerable membrane remodeling (for example Epithelial Mesenchymal Transition during tumor metastasis) or that involve misfolded protein aggregates in endosomal compartments (59, 60).

MATERIALS AND METHODS

Strains and Genetic Methods

Standard methods were used for growth and genetic analysis of worms (61). Integration of plasmid DNA was done by microparticle bombardment into *unc-119(ed3)* worms as previously described, except that we used plasmids pHD134 or pHD137 as co-bombardment markers; in addition to wild type *C. elegans unc-119*, pHD134 and pHD137 were engineered to also include p*ttx-3::GFP* and a p*myo-2::GFP*, respectively (18, 62). Markers used: *cup-2(ar506) I* (32), *rme-1(b1045) V* (33), *cup-5(ar465) III* (34); *snx-1(tm847) X* (29). *zcIs4[hsp-4::GFP] V* transgene expresses GFP under the control of the *hsp-4* promoter (63); t h e *arIs37[*p*myo-3::ssGFP] I* transgene is used to visualize endocytosis by coelomocytes of GFP expressed and secreted by body wall muscle cells into the body cavity (32); *cdIs70[pcc1::GFP::MCA-3c; unc-1119(+)*-p*myo-2::GFP]* expresses a functional GFP-MCA-3 in coelomocytes and soluble GFP in the pharynx (18).

HeLa cells and murine RAW264.7 macrophages (ATCC, Manassas, VA) were grown in Dulbecco's Modified Eagle Medium (DMEM) containing 2 mM Glutamax and supplemented with 10% Fetal Bovine Serum, 100 U/ml penicillin, and 100 μg/ml streptomycin (Invitrogen, Carlsbad, CA) at 37° in 95% air at 5% carbon dioxide. RAW264.7 sable clones expressing Derlin-1-GFP or Derlin-1 shRNA were previously described and were grown in the same medium supplemented with 250 μg/ml G418 (18).

Molecular Methods

Standard methods were used for the manipulation of recombinant DNA (64). Polymerase chain reaction (PCR) was done using the Expand Long Template PCR System (Boehringer Manheim, Manheim, Germany) according to the manufacturer's instructions. All other enzymes were from New England Biolabs (Ipswich, MA), unless otherwise indicated.

Plasmids

The following plasmids were made for this study (listed in order of use):

- pHD290: GAL4p DNA Binding Domain fused to carboxyl terminus of *C. elegans* SNX-1 for yeast two-hybrid studies.

- pHD297: GAL4p Activation Domain fused to carboxyl terminus of *C. elegans* CUP-2 for yeast two-hybrid studies.

- pHD291: GAL4p Activation Domain fused to carboxyl terminus of *C. elegans* R151.6 for yeast two-hybrid studies.

- pHD403: Cub-LexA-VP16 fused to carboxyl terminus of *C. elegans* R151.6 for split-ubiquitin yeast two-hybrid studies.

- pHD404: Cub-LexA-VP16 fused to carboxyl terminus of *C. elegans* CUP-2 for split-ubiquitin yeast two-hybrid studies.

- pHD380: NubG fused to carboxyl terminus of *C. elegans* CUP-2 for split-ubiquitin yeast two-hybrid studies.

- pHD381: NubG fused to carboxyl terminus of *C. elegans* R151.6 for split-ubiquitin yeast two-hybrid studies.

- pHD389: NubG fused to amino terminus of *C. elegans* SNX-1 for split-ubiquitin yeast two-hybrid studies.

- pHD275: *C. elegans* CUP-2 with carboxyl terminus-fused 3X FLAG epitope under the control of the *cup-2* promoter.

- pHD406: Cub-LexA-VP16 fused to carboxyl terminus of mouse Derlin-1 for split-ubiquitin yeast two-hybrid studies.

- pHD412: Cub-LexA-VP16 fused to carboxyl terminus of mouse Derlin-2 for split-ubiquitin yeast two-hybrid studies.

- pHD388: NubG fused to amino terminus of mouse Derlin-1 for split-ubiquitin yeast two-hybrid studies.

- pHD377: NubG fused to amino terminus of mouse Derlin-2 for split-ubiquitin yeast two-hybrid studies.

- pHD390: NubG fused to amino terminus of mouse Snx1 for split-ubiquitin yeast two-hybrid studies.

- pHD408: NubG fused to amino terminus of mouse Snx2 for split-ubiquitin yeast two-hybrid studies.

- pHD396: NubG fused to amino terminus of mouse Snx4 for split-ubiquitin yeast two-hybrid studies.

- pHD298: GFP fused to carboxyl terminus of mouse Derlin-1 for mammalian expression.

- pHD673: 3xFLAG epitope fused to amino terminus of mouse Snx1 for mammalian expression.

- pHD672: 3xFLAG epitope fused to amino terminus of mouse Snx2 for mammalian expression.

- pHD679: 3xFLAG epitope fused to amino terminus of mouse Snx4 for mammalian expression.

Details of plasmid constructions are available upon request.

Analysis of Markers for Various Coelomocyte Compartments

We took confocal images of coelomocytes in young adult hermaphrodites grown at the various temperatures to quantitate the fluorescence from GFP-fused markers in various backgrounds. The images were taken using the same microscopy parameters. Images were analyzed using Adobe Photoshop (Adobe Systems Incorporated, San Jose, CA) or Metamorph software (Molecular Devices, Sunnyvale, CA) to measure sizes of compartments and fluorescence intensities. For all quantitations, the reported values reflect the average from at least 60 measurements. The bars on the charts represent standard deviations.

Yeast Two-Hybrid Analyses

Conventional yeast two-hybrid studies using GAL4p DNA Binding and Activation domain fusions were done as previously described (65).

Split-ubiquitin yeast two-hybrid assays were done using the Dualsystems Biotech kit (Switzerland). Fusion plasmids were transformed into the yeast strain NMY51 [MATa his3delta200 trp1-901 leu2-3,112 ade2 LYS2::(lexAop)4-HIS3 ura3::(lexAop)8-lacZ (lexAop)8-ADE2 GAL4)] and selected on –leu –trp plates. Equal numbers of cells from each transformation were spotted on –leu –trp and –leu –trp –ade –his + 5 mM 3-AT plates that were placed at 30°. Growth was scored over the next four days.

Worm Immunoprecipitation

We resuspended 2-4 ml of packed adult hermaphrodites in 20 ml of buffer D (20 mM Tris-HCl pH 8.0, 10% glycerol, 150 mM NaCl) after washing the worms with this buffer. We then added β-mercaptoethanol to a final concentration of 7 mM and 200 μl of a solution of protease inhibitors per 10 ml of worm suspension (Sigma-Aldrich, St. Louis, MO). Worms were homogenized by french pressing three times at 1000-1400 psi (ratio “high”) and then centrifuged at 5000 rpm for 10 minutes. The supernatant was centrifuged at 125,000*g* for two hours and the pellet was resuspended in 10 ml of buffer D with β-mercaptoethanol and protease inhibitors and adjusted to 1% Triton X-100. The pellet was homogenized using a dounce homogenizer, allowed to stir for 2 hours at 4°, centrifuged at 35,000*g* for 30 minutes, and the supernatant was dialyzed twice, two hours each time, in 2 liters of IPP50 (20 mM Tris-HCl pH 8.0, 150 mM NaCl, 0.05% Triton X-100). 10 μl of 1-5 mg/ml antibody, and 200 μl of Protein A/G agarose beads (Pierce Biotechnology, Rockford, IL) pre-washed with IPP150 were added to 4 ml of this solution for each immunoprecipitation. After overnight incubation at 4°, the beads were washed four times with 50 mM Hepes 7.7, 150 mM NaCl, 1% NP-40. To elute, beads were incubated in 100 μl 1x SDS buffer (50 mM Tris-HCl pH 8.5, 1% SDS, 2 mM DTT) for 5 minutes at 95°. The beads were centrifuged at 2000 rpm for 1 minute and 80 μl were recovered. This procedure was repeated with 70 μl SDS buffer added to the beads. This time, 70 μl was recovered and mixed with the previous 80 μl. 150 μl of 2x Western loading buffer was added, and the mixture was incubated at 95° for 10 minutes before loading on a gel.

Quantitation of GFP::MCA-3 Bands on Western Blots

Equal volumes of samples were run on gels and probed with a goat anti-GFP antibody conjugated to HRP (Research Diagnostics Inc, Concord, MA). Since the GFP::MCA-3 transgene also expresses GFP in the pharynx, we used it as an internal control. In each lane, we measured the intensity of the GFP::MCA-3 band and divided it by the intensity of the GFP band to give us a normalized measurement. Samples were run three times to ensure reproducibility. Measurements were done using ImageJ software (N.I.H., Bethesda, MD).

Mammalian Immunoprecipitation

We grew ten 100 mm plates of RAW264.7 to 80% confluence. Each plate was washed twice with ice-cold PBS, and the cells were scraped off each plate in 0.6 ml of ice-cold Lysis buffer (20 mM Tris pH 7.5, 150 mM NaCl, 1% NP40, 5 mM EDTA, 0.42 mg/ml sodium fluoride, 0.368 mg/ml sodium orthovanadate, 0.0121 mg/ml ammonium molybdate, 0.04 Complete protease inhibitors tablet/ml (Roche Diagnostics, Mannheim, Germany). The lysates were combined and allowed to mix for 20 minutes at 4°, and the supernatant from a 15-minute, ~11,000g spin at 4° was kept at -80° until further use.

Immunoprecipitations were done by adding 10 μg of each antibody to 100 μl of lysate mixed with 850 μl of TNEN buffer (same as Lysis Buffer but with 0.5% NP-40) and mixing for 1 hour at 4°. This mixture was added to columns that contained 50 μl Protein A/G agarose beads that had been pre-washed with Lysis buffer. The columns were capped and left to mix overnight at 4°. The beads were then washed three times with 10 ml of ice-cold TNEN buffer each time and eluted using 200 μl of a low pH elution buffer (Pierce). The eluate was neutralized using 1 M Tris, pH 9.5 (1:100 dilution), and 50 μl of 5x Western loading buffer was added. The mixtures were incubated at 95° for 10 minutes before loading on a gel.

Derlin-GFP Immunoprecipitation and Mass Spectrometry

We immunoprecipitated Derlin-1-GFP from lysates of RAW264.7 macrophages stably expressing Derlin-1-GFP using bead-conjugated anti-GFP antibody (MBL, Woburn, MA) (18). We then identified proteins that co-immunoprecipitated using MudPIT analysis (66, 67). To reduce the identification of non-specific co-purifying proteins, we did the same procedure on stable RAW264.7 clones we made that express the integral membrane protein GFPTRPML1 (38). Samples were subjected to Mass Spectrometry three times to identify >90% of the proteins in each of the samples. Proteins in each sample were identified with an identification probability greater than 90% using the Scaffold program (68-70). Proteins that were identified in the Derlin-1-GFP sample but not in the GFP-TRPML1 sample were considered candidate Derlin-1-specific interactors.

RAW264.7 Immunofluorescence

For conventional immunofluorescence, cells that were grown on coverslips were fixed for 20 minutes in 4% paraformaldehyde in PBS at 24° or in 100% MetOH (kept at -20°) for 15 minutes at -20°. Cells were washed three times with PBS at 24°, 5 minutes each time. Paraformaldehyde-fixed cells were incubated in 50 mM NH_4Cl in PBS for 10 minutes at 24° and washed two more times with PBS. Blocking was done for 30 min in blocking buffer (1% BSA, 0.1% Saponin, in PBS). Cells were then incubated in primary antibodies diluted

in blocking buffer for two hours at 24°, washed three times with PBS, incubated in Cy2 or Cy3 labeled secondary antibodies (Jackson ImmunoResearch Laboratories, West Grove, PA) diluted 1:200 in blocking buffer for one hour at 24°, washed three times with PBS, and mounted in Slowfade mounting medium (Invitrogen) on slides for viewing.

Microscopy

Confocal images were taken with a Nikon PCM 2000, using HeNe 543 excitation for the red dye and Argon 488 for the green dye. Deconvolution Images were acquired (100x, 1.4 NA objective, 0.2 mm z-sections) on a DeltaVision RT system (Applied Precision, LLC, Issaquah, WA) using a Series 300 CCD camera (Photometrics, Tucson, AZ) and deconvolved using DeltaVision software. For *C. elegans* imaging, young adult hermaphrodites were paralyzed in 10 mM levamisole.

Ricin Sulfation Assay

RS1, a ricin variant containing a modified ricin A chain with a tyrosine sulfation site (ricin A-sulf$_1$) and reconstituted with ricin B chain, was produced and purified as previously described (51). Cells were washed twice with sulfate-free DMEM supplemented with 2 mM L-glutamine, followed by incubation with 0.2 mCi/ml $H_2{}^{35}SO_4$ (Hartman Analytic, Braunschweig, Germany) in sulfate-free DMEM for 3 hours at 37°. For Misfolding Buffer-1 (MFB-1) treatment, the medium was removed and ice-cold MFB-1 (741 mM citric acid, 258.7 mM sodium citrate, pH 3.5) or PBS as control was added to the cells for 5 minutes on ice. After one wash with PBS, the cells were washed twice with sulfate-free DMEM and RS1 was added to a final concentration of 6 μg/ml in sulfate-free DMEM containing 0.2 mCi/ml $H_2{}^{35}SO_4$ and incubated for 2 hours at 37°. For experiments that did not include MFB-1 treatment, RS1 was added directly to the cells after 3 hours pre-incubation with $H\ {}^{35}{}_2SO_4$-containing DMEM. After RS1-incubation, the medium was removed and the cells were washed twice with 0.1 M lactose to remove surface-bound RS1, and once in PBS, before addition of 400 μl lysis buffer [0.1 M NaCl, 10 mM Na_2HPO_4, 1 mM EDTA, 1 % Triton X-100, 60 mM octyl-glucopyranoside] supplemented with Complete protease inhibitors. The lysate was cleared by centrifugation (8000 rpm, 10 minutes) and RS1 was immunoprecipitated with anti-ricin antibody (Sigma Aldrich, St. Louis, MO, USA) pre-bound to Protein ASepharose beads (Amersham Biosciences, Buckinghamshire, UK) overnight at 4°. The precipitate was separated by SDS-PAGE under reducing conditions, and blotted onto a PVDF membrane (Immobilon-P, Millipore, Billerica, MA, USA). The bands were detected by autoradiography and imaged and quantified using PharosFX scanner and QuantityOne software (BioRad Laboratories Inc, Hercules, CA, USA). The total amount of sulfated proteins was determined by TCA-precipitation of all ^{35}S-labeled proteins in the lysates.

Ricin Western Blot

After the sulfation assay, the membrane was re-wet in PBS-T (PBS + 0.01% Tween-20) for 30 minutes, before an anti-ricin antibody (Sigma Aldrich, St. Louis, MO, USA) in 2.5% reconstituted skim milk (RSM) was applied overnight at 4°. After 3×5 minutes washes in PBS-T, an HRP-linked anti-rabbit antibody (Jackson Laboratories, Maine, USA) in 2.5%

RSM was applied for 1 hour at room temperature. After 3×5 minutes washes in PBS-T, ImmuneStar substrate (BioRad Laboratories Inc, Hercules, CA, USA) was applied for 1 minute. The signal was detected and quantified using BioRad Imager and ImageLab software (BioRad Laboratories Inc, Hercules, CA, USA).

Ricin Cytotoxicity Assays

Cell lines were seeded in 24-well plates at a concentration of 5×10^4 cells/well two days before the experiment. The cells were washed twice in leucine-free Hepes medium before increasing concentrations of ricin was added [1-1000 ng/ml], and the cells incubated for 3 hours. The medium was then replaced with leucine-free Hepes-medium containing 2 μCi/ml [^{3}H]leucine, and the cells incubated further for 20 minutes. The proteins were precipitated with 5% TCA, washed once in 5% TCA, and then dissolved in 0.1 M KOH. The incorporation of radioactivity-labeled leucine was quantified, and toxicity curves generated for each cell line. IC50 was calculated as the concentration of ricin giving a 50% reduction in protein synthesis, and fold protection was determined as the ratio between the IC50 for the Derlin-1 cell lines compared to the parental cell line.

Alternatively, RAW264.7 cells were added to 96-well plates at a concentration of 4×10^5 cells/well and left for two days. After Misfolding Buffer-1 (MFB-1) or PBS treatment for 5 minutes at 4°, cells were washed once with ice-cold PBS and twice with ice-cold DMEM medium. Cells were then incubated for 24 hours in DMEM medium in the presence of various concentrations of ricin. Viability was determined using the MTT assay (71, 72). Each assay was done in triplicate to calculate averages and standard deviations.

Additional Antibodies Used

Antibodies used were mouse anti-FLAG M2 monoclonal (Sigma-Aldrich), rabbit anti-Derlin-1 (MBL International, Woburn, MA), rabbit anti-Derlin-2 (MBL International), rabbit anti-Snx1 (Abcam, Cambridge, UK), chicken anti-Snx2 (Abcam), goat anti-Snx4 (Santa Cruz Biotechnology, Santa Cruz, CA), and rabbit anti-Destrin (GeneTex, San Antonio, TX).

For antigen detection, we used Goat anti-Rabbit IgG, Rabbit anti-Chicken IgY, and Swine anti-Goat IgG secondary antibodies conjugated to HRP (1:50,000) and the SuperSignal West Dura Extended Duration Substrate (Pierce).

Statistical Methods

Student t test was used to compare average measurements from two samples using a two-tailed distribution (Tails = 2) and a two-sample unequal variance (Type = 2).

Supplementary Material

Refer to Web version on PubMed Central for supplementary material.

ACKNOWLEDGEMENTS

We thank Shohei Mitani and the National Bioresource Project for the Experimental Animal "Nematode *C. elegans*" for the *tm* allele deletion worms and Chonglin Yang for backcrossed *C. elegans* retromer mutants. Some nematode strains used in this work were provided by the Caenorhabditis Genetics Center, which is funded by the NIH National Center for Research Resources. We thank Hidde Ploegh for GFP-tagged human Derlin expression vectors and Peter Cullen for FLAG-tagged human Snx and Retromer expression vectors. We also thank Anne-Grethe Myrann for expert technical assistance. This work was supported by grants from the Norwegian Cancer Society, the Norwegian Research Council and the Norwegian South-Eastern Health Authority to T.I.K and K.S. and an Arizona Biomedical Research Commission grant 8-006 to H. F.

REFERENCES

1. Goldberg AL. Protein degradation and protection against misfolded or damaged proteins. Nature. 2003; 426(6968):895–899. [PubMed: 14685250]
2. Meusser B, Hirsch C, Jarosch E, Sommer T. ERAD: the long road to destruction. Nat Cell Biol. 2005; 7(8):766–772. [PubMed: 16056268]
3. von Mikecz A. The nuclear ubiquitin-proteasome system. J Cell Sci. 2006; 119(Pt 10):1977–1984. [PubMed: 16687735]
4. Meyer HA, Grau H, Kraft R, Kostka S, Prehn S, Kalies KU, Hartmann E. Mammalian Sec61 is associated with Sec62 and Sec63. J Biol Chem. 2000; 275(19):14550–14557. [PubMed: 10799540]
5. Raden D, Song W, Gilmore R. Role of the cytoplasmic segments of Sec61alpha in the ribosome-binding and translocation-promoting activities of the Sec61 complex. J Cell Biol. 2000; 150(1):53–64. [PubMed: 10893256]
6. Maattanen P, Gehring K, Bergeron JJ, Thomas DY. Protein quality control in the ER: the recognition of misfolded proteins. Semin Cell Dev Biol. 2010; 21(5):500–511. [PubMed: 20347046]
7. Vembar SS, Brodsky JL. One step at a time: endoplasmic reticulum-associated degradation. Nat Rev Mol Cell Biol. 2008; 9(12):944–957. [PubMed: 19002207]
8. Pilon M, Schekman R, Romisch K. Sec61p mediates export of a misfolded secretory protein from the endoplasmic reticulum to the cytosol for degradation. Embo J. 1997; 16(15):4540–4548. [PubMed: 9303298]
9. Plemper RK, Bohmler S, Bordallo J, Sommer T, Wolf DH. Mutant analysis links the translocon and BiP to retrograde protein transport for ER degradation. Nature. 1997; 388(6645):891–895. [PubMed: 9278052]
10. Plemper RK, Bordallo J, Deak PM, Taxis C, Hitt R, Wolf DH. Genetic interactions of Hrd3p and Der3p/Hrd1p with Sec61p suggest a retro-translocation complex mediating protein transport for ER degradation. J Cell Sci. 1999; 112(Pt 22):4123–4134. [PubMed: 10547371]
11. Schekman R. Cell biology: a channel for protein waste. Nature. 2004; 429(6994):817–818. [PubMed: 15215847]
12. Wahlman J, DeMartino GN, Skach WR, Bulleid NJ, Brodsky JL, Johnson AE. Real-time fluorescence detection of ERAD substrate retrotranslocation in a mammalian in vitro system. Cell. 2007; 129(5):943–955. [PubMed: 17540174]
13. Wiertz EJ, Tortorella D, Bogyo M, Yu J, Mothes W, Jones TR, Rapoport TA, Ploegh HL. Sec61-mediated transfer of a membrane protein from the endoplasmic reticulum to the proteasome for destruction. Nature. 1996; 384(6608):432–438. [PubMed: 8945469]
14. Zhou M, Schekman R. The engagement of Sec61p in the ER dislocation process. Mol Cell. 1999; 4(6):925–934. [PubMed: 10635318]
15. Apaja PM, Xu H, Lukacs GL. Quality control for unfolded proteins at the plasma membrane. J Cell Biol. 2010 in press.
16. Benharouga M, Haardt M, Kartner N, Lukacs GL. COOH-terminal truncations promote proteasome-dependent degradation of mature cystic fibrosis transmembrane conductance regulator from post-Golgi compartments. J Cell Biol. 2001; 153(5):957–970. [PubMed: 11381082]

17. Ljunggren HG, Stam NJ, Ohlen C, Neefjes JJ, Hoglund P, Heemels MT, Bastin J, Schumacher TN, Townsend A, Karre K, et al. Empty MHC class I molecules come out in the cold. Nature. 1990; 346(6283):476–480. [PubMed: 2198471]
18. Schaheen B, Dang H, Fares H. Derlin-dependent accumulation of integral membrane proteins at cell surfaces. J Cell Sci. 2009; 122(Pt 13):2228–2239. [PubMed: 19509052]
19. Sharma M, Pampinella F, Nemes C, Benharouga M, So J, Du K, Bache KG, Papsin B, Zerangue N, Stenmark H, Lukacs GL. Misfolding diverts CFTR from recycling to degradation: quality control at early endosomes. J Cell Biol. 2004; 164(6):923–933. [PubMed: 15007060]
20. Wilson MH, Highfield HA, Limbird LE. The role of a conserved inter-transmembrane domain interface in regulating alpha(2a)-adrenergic receptor conformational stability and cell-surface turnover. Mol Pharmacol. 2001; 59(4):929–938. [PubMed: 11259639]
21. Okiyoneda T, Barriere H, Bagdany M, Rabeh WM, Du K, Hohfeld J, Young JC, Lukacs GL. Peripheral protein quality control removes unfolded CFTR from the plasma membrane. Science. 2010; 329(5993):805–810. [PubMed: 20595578]
22. Carlton J, Bujny M, Rutherford A, Cullen P. Sorting nexins--unifying trends and new perspectives. Traffic. 2005; 6(2):75–82. [PubMed: 15634208]
23. Worby CA, Dixon JE. Sorting out the cellular functions of sorting nexins. Nat Rev Mol Cell Biol. 2002; 3(12):919–931. [PubMed: 12461558]
24. Arighi CN, Hartnell LM, Aguilar RC, Haft CR, Bonifacino JS. Role of the mammalian retromer in sorting of the cation-independent mannose 6-phosphate receptor. J Cell Biol. 2004; 165(1):123–133. [PubMed: 15078903]
25. Carlton J, Bujny M, Peter BJ, Oorschot VM, Rutherford A, Mellor H, Klumperman J, McMahon HT, Cullen PJ. Sorting nexin-1 mediates tubular endosometo-TGN transport through coincidence sensing of high- curvature membranes and 3-phosphoinositides. Curr Biol. 2004; 14(20):1791–1800. [PubMed: 15498486]
26. Seaman MN. Cargo-selective endosomal sorting for retrieval to the Golgi requires retromer. J Cell Biol. 2004; 165(1):111–122. [PubMed: 15078902]
27. Utskarpen A, Slagsvold HH, Dyve AB, Skanland SS, Sandvig K. SNX1 and SNX2 mediate retrograde transport of Shiga toxin. Biochem Biophys Res Commun. 2007; 358(2):566–570. [PubMed: 17498660]
28. Schwarz DG, Griffin CT, Schneider EA, Yee D, Magnuson T. Genetic analysis of sorting nexins 1 and 2 reveals a redundant and essential function in mice. Mol Biol Cell. 2002; 13(10):3588–3600. [PubMed: 12388759]
29. Shi A, Sun L, Banerjee R, Tobin M, Zhang Y, Grant BD. Regulation of endosomal clathrin and retromer-mediated endosome to Golgi retrograde transport by the J-domain protein RME-8. Embo J. 2009; 28(21):3290–3302. [PubMed: 19763082]
30. Li S, Armstrong CM, Bertin N, Ge H, Milstein S, Boxem M, Vidalain PO, Han JD, Chesneau A, Hao T, Goldberg DS, Li N, Martinez M, Rual JF, Lamesch P, et al. A map of the interactome network of the metazoan *C. elegans*. Science. 2004; 303(5657):540–543. [PubMed: 14704431]
31. Iyer K, Burkle L, Auerbach D, Thaminy S, Dinkel M, Engels K, Stagljar I. Utilizing the split-ubiquitin membrane yeast two-hybrid system to identify protein-protein interactions of integral membrane proteins. Sci STKE. 2005; 2005(275):pl3. [PubMed: 15770033]
32. Fares H, Greenwald I. Genetic analysis of endocytosis in *Caenorhabditis elegans*: coelomocyte uptake defective mutants. Genetics. 2001; 159(1):133–145. [PubMed: 11560892]
33. Grant B, Zhang Y, Paupard MC, Lin SX, Hall DH, Hirsh D. Evidence that RME-1, a conserved *C. elegans* EH-domain protein, functions in endocytic recycling. Nat Cell Biol. 2001; 3(6):573–579. [PubMed: 11389442]
34. Fares H, Greenwald I. Regulation of endocytosis by CUP-5, the *Caenorhabditis elegans* mucolipin-1 homolog. Nat Genet. 2001; 28(1):64–68. [PubMed: 11326278]
35. Treusch S, Knuth S, Slaugenhaupt SA, Goldin E, Grant BD, Fares H. *Caenorhabditis elegans* functional orthologue of human protein h-mucolipin-1 is required for lysosome biogenesis. Proc Natl Acad Sci U S A. 2004; 101(13):4483–4488. [PubMed: 15070744]
36. Bonifacino JS, Hurley JH. Retromer. Curr Opin Cell Biol. 2008; 20(4):427–436. [PubMed: 18472259]

37. Wassmer T, Attar N, Harterink M, van Weering JR, Traer CJ, Oakley J, Goud B, Stephens DJ, Verkade P, Korswagen HC, Cullen PJ. The retromer coat complex coordinates endosomal sorting and dynein-mediated transport, with carrier recognition by the trans-Golgi network. Dev Cell. 2009; 17(1):110–122. [PubMed: 19619496]

38. Thompson EG, Schaheen L, Dang H, Fares H. Lysosomal trafficking functions of mucolipin-1 in murine macrophages. BMC Cell Biol. 2007; 8:54. [PubMed: 18154673]

39. Bernardi KM, Forster ML, Lencer WI, Tsai B. Derlin-1 facilitates the retrotranslocation of cholera toxin. Mol Biol Cell. 2008; 19(3):877–884. [PubMed: 18094046]

40. Nishitoh H, Kadowaki H, Nagai A, Maruyama T, Yokota T, Fukutomi H, Noguchi T, Matsuzawa A, Takeda K, Ichijo H. ALS-linked mutant SOD1 induces ER stress- and ASK1-dependent motor neuron death by targeting Derlin-1. Genes Dev. 2008; 22(11):1451–1464. [PubMed: 18519638]

41. Ye Y, Shibata Y, Kikkert M, van Voorden S, Wiertz E, Rapoport TA. Inaugural Article: Recruitment of the p97 ATPase and ubiquitin ligases to the site of retrotranslocation at the endoplasmic reticulum membrane. Proc Natl Acad Sci U S A. 2005; 102(40):14132–14138. [PubMed: 16186510]

42. Younger JM, Chen L, Ren HY, Rosser MF, Turnbull EL, Fan CY, Patterson C, Cyr DM. Sequential quality-control checkpoints triage misfolded cystic fibrosis transmembrane conductance regulator. Cell. 2006; 126(3):571–582. [PubMed: 16901789]

43. Haft CR, de la Luz Sierra M, Bafford R, Lesniak MA, Barr VA, Taylor SI. Human orthologs of yeast vacuolar protein sorting proteins Vps26, 29, and 35: assembly into multimeric complexes. Mol Biol Cell. 2000; 11(12):4105–41016. [PubMed: 11102511]

44. Nishida E, Muneyuki E, Maekawa S, Ohta Y, Sakai H. An actin-depolymerizing protein (destrin) from porcine kidney. Its action on F-actin containing or lacking tropomyosin. Biochemistry. 1985; 24(23):6624–6630. [PubMed: 4084546]

45. Lilley BN, Ploegh HL. Multiprotein complexes that link dislocation, ubiquitination, and extraction of misfolded proteins from the endoplasmic reticulum membrane. Proc Natl Acad Sci U S A. 2005; 102(40):14296–14301. [PubMed: 16186509]

46. Sandvig K, Torgersen ML, Engedal N, Skotland T, Iversen TG. Protein toxins from plants and bacteria: probes for intracellular transport and tools in medicine. FEBS Lett. 2010; 584(12):2626–2634. [PubMed: 20385131]

47. Sandvig K, Spilsberg B, Lauvrak SU, Torgersen ML, Iversen TG, van Deurs B. Pathways followed by protein toxins into cells. Int J Med Microbiol. 2004; 293(7-8):483–490. [PubMed: 15149022]

48. Sandvig K, van Deurs B. Transport of protein toxins into cells: pathways used by ricin, cholera toxin and Shiga toxin. FEBS Lett. 2002; 529(1):49–53. [PubMed: 12354612]

49. Dyve AB, Bergan J, Utskarpen A, Sandvig K. Sorting nexin 8 regulates endosome-to-Golgi transport. Biochem Biophys Res Commun. 2009; 390(1):109–114. [PubMed: 19782049]

50. Skanland SS, Walchli S, Utskarpen A, Wandinger-Ness A, Sandvig K. Phosphoinositide-regulated retrograde transport of ricin: crosstalk between hVps34 and sorting nexins. Traffic. 2007; 8(3): 297–309. [PubMed: 17319803]

51. Rapak A, Falnes PO, Olsnes S. Retrograde transport of mutant ricin to the endoplasmic reticulum with subsequent translocation to cytosol. Proc Natl Acad Sci U S A. 1997; 94(8):3783–3788. [PubMed: 9108055]

52. Lilley BN, Ploegh HL. A membrane protein required for dislocation of misfolded proteins from the ER. Nature. 2004; 429(6994):834–840. [PubMed: 15215855]

53. Schroder M, Kaufman RJ. ER stress and the unfolded protein response. Mutat Res. 2005; 569(1-2): 29–63. [PubMed: 15603751]

54. Slominska-Wojewodzka M, Gregers TF, Walchli S, Sandvig K. EDEM is involved in retrotranslocation of ricin from the endoplasmic reticulum to the cytosol. Mol Biol Cell. 2006; 17(4):1664–1675. [PubMed: 16452630]

55. Ackerman AL, Kyritsis C, Tampe R, Cresswell P. Access of soluble antigens to the endoplasmic reticulum can explain cross-presentation by dendritic cells. Nat Immunol. 2005; 6(1):107–113. [PubMed: 15592474]

56. Teter K, Holmes RK. Inhibition of endoplasmic reticulum-associated degradation in CHO cells resistant to cholera toxin, Pseudomonas aeruginosa exotoxin A, and ricin. Infect Immun. 2002; 70(11):6172–6179. [PubMed: 12379695]
57. Maxfield FR, McGraw TE. Endocytic recycling. Nat Rev Mol Cell Biol. 2004; 5(2):121–132. [PubMed: 15040445]
58. Zaliauskiene L, Kang S, Brouillette CG, Lebowitz J, Arani RB, Collawn JF. Down-regulation of cell surface receptors is modulated by polar residues within the transmembrane domain. Mol Biol Cell. 2000; 11(8):2643–2655. [PubMed: 10930460]
59. Thiery JP, Huang R. Linking epithelial-mesenchymal transition to the well-known polarity protein Par6. Dev Cell. 2005; 8(4):456–458. [PubMed: 15809027]
60. Vieira SI, Rebelo S, Esselmann H, Wiltfang J, Lah J, Lane R, Small SA, Gandy S, da Cruz ESEF, da Cruz ESOA. Retrieval of the Alzheimer's amyloid precursor protein from the endosome to the TGN is S655 phosphorylation state-dependent and retromer-mediated. Mol Neurodegener. 2010; 5(1):40. [PubMed: 20937087]
61. Brenner S. The genetics of *Caenorhabditis elegans*. Genetics. 1974; 77(1):71–94. [PubMed: 4366476]
62. Praitis V. Creation of transgenic lines using microparticle bombardment methods. Methods Mol Biol. 2006; 351:93–107. [PubMed: 16988428]
63. Calfon M, Zeng H, Urano F, Till JH, Hubbard SR, Harding HP, Clark SG, Ron D. IRE1 couples endoplasmic reticulum load to secretory capacity by processing the XBP-1 mRNA. Nature. 2002; 415(6867):92–96. [PubMed: 11780124]
64. Sambrook, J.; Fritch, EF.; Maniatis, T. Molecular cloning: a laboratory manual. 2nd edition. Cold Spring Harbor Laboratory; Cold Spring Harbor, NY: 1989.
65. James P, Halladay J, Craig EA. Genomic libraries and a host strain designed for highly efficient two-hybrid selection in yeast. Genetics. 1996; 144(4):1425–1436. [PubMed: 8978031]
66. Chen EI, Hewel J, Felding-Habermann B, Yates JR 3rd. Large scale protein profiling by combination of protein fractionation and multidimensional protein identification technology (MudPIT). Mol Cell Proteomics. 2006; 5(1):53–56. [PubMed: 16272560]
67. Liu H, Lin D, Yates JR 3rd. Multidimensional separations for protein/peptide analysis in the post-genomic era. Biotechniques. 2002; 32(4):898, 900, 902. passim. [PubMed: 11962611]
68. Craig R, Beavis RC. TANDEM: matching proteins with tandem mass spectra. Bioinformatics. 2004; 20(9):1466–1467. [PubMed: 14976030]
69. Keller A, Nesvizhskii AI, Kolker E, Aebersold R. Empirical statistical model to estimate the accuracy of peptide identifications made by MS/MS and database search. Anal Chem. 2002; 74(20):5383–5392. [PubMed: 12403597]
70. Nesvizhskii AI, Keller A, Kolker E, Aebersold R. A statistical model for identifying proteins by tandem mass spectrometry. Anal Chem. 2003; 75(17):4646–4658. [PubMed: 14632076]
71. Cory AH, Owen TC, Barltrop JA, Cory JG. Use of an aqueous soluble tetrazolium/formazan assay for cell growth assays in culture. Cancer Commun. 1991; 3(7):207–212. [PubMed: 1867954]
72. Mosmann T. Rapid colorimetric assay for cellular growth and survival: application to proliferation and cytotoxicity assays. J Immunol Methods. 1983; 65(1-2):55–63. [PubMed: 6606682]

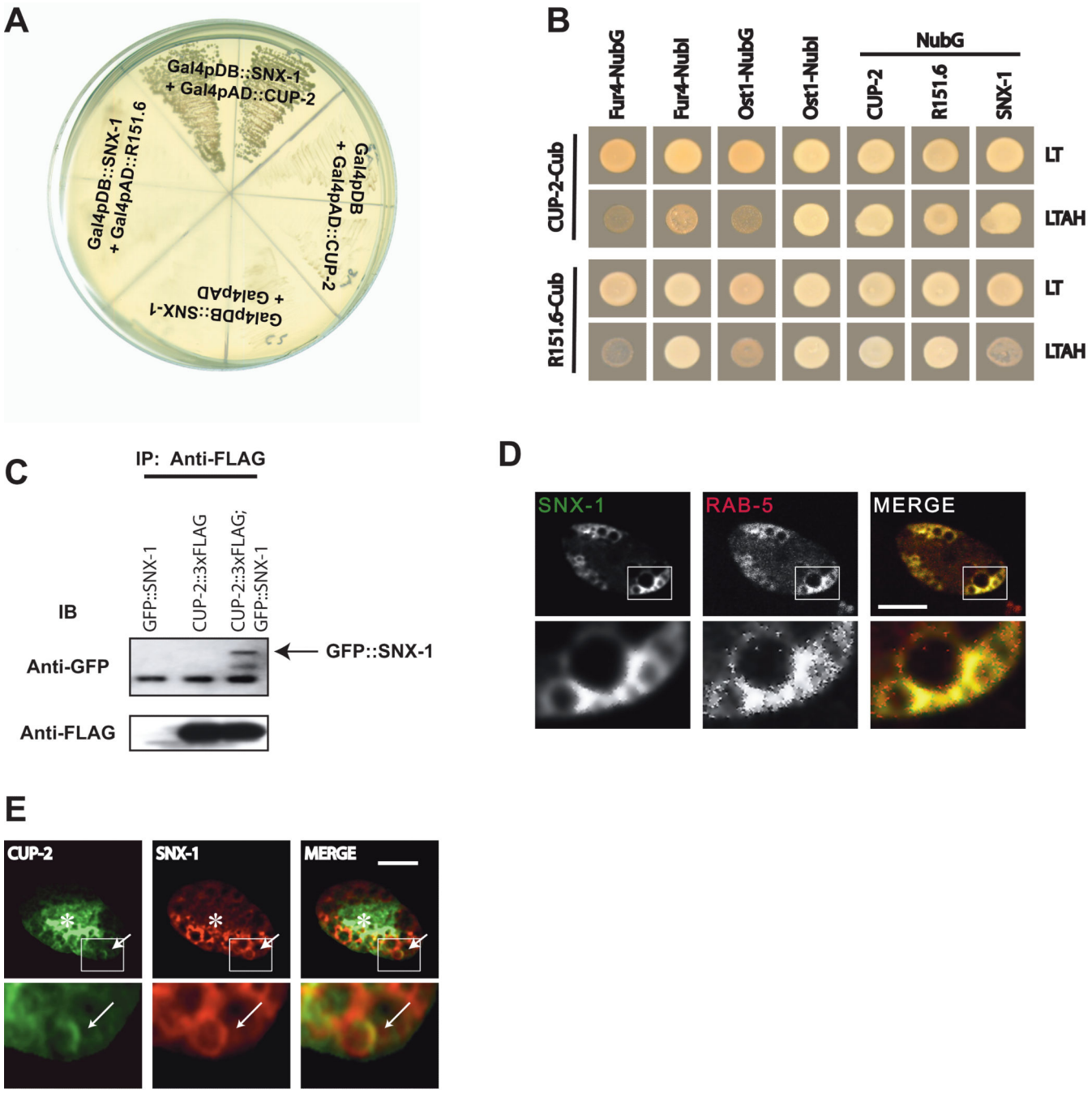

Figure 1. *C. elegans* Derlin and Sorting Nexin Physical Association

A) Conventional yeast two-hybrid assay using the indicated constructs. The image shows growth on –leu –trp –ade –his + 5 mM 3-AT plates after four days at 30°. B) Split-ubiquitin yeast two-hybrid assay using CUP-2-Cub and R151.6-Cub-expressing plasmids. The same number of yeast cells were spotted on –leu –trp (LT) plates to monitor growth without selection and on – leu –trp –ade –his + 5 mM 3-AT (LHAT) to assay physical interactions. The image is after three days of growth at 30°. C) Western blots using anti-GFP or anti-FLAG antibodies after immunoprecipitation with Anti-FLAG antibodies.

Immunoprecipitation was done on membrane preparations from the indicated strains expressing GFP::SNX-1, CUP-2::FLAG, or both. These strains were also homozygous for *cup-2(ar506)*. D) Confocal images of coelomocytes in adult worms co-expressing GFP::SNX-1 and mCherry::RAB-5. The bottom row shows a higher magnification image of the boxed area in the upper row. Bar is 5 μm in upper row and 1 μm in lower row images. E) Deconvolution images of a coelomocyte expressing CUP-2::GFP (green) and mRFP::SNX-1 (red). The bottom row shows a higher magnification image of the boxed area in the upper row. Arrows indicate co-localization. Asterisks indicate ER. Bar is 5 μm in upper row and 1.5 μm in lower row images.

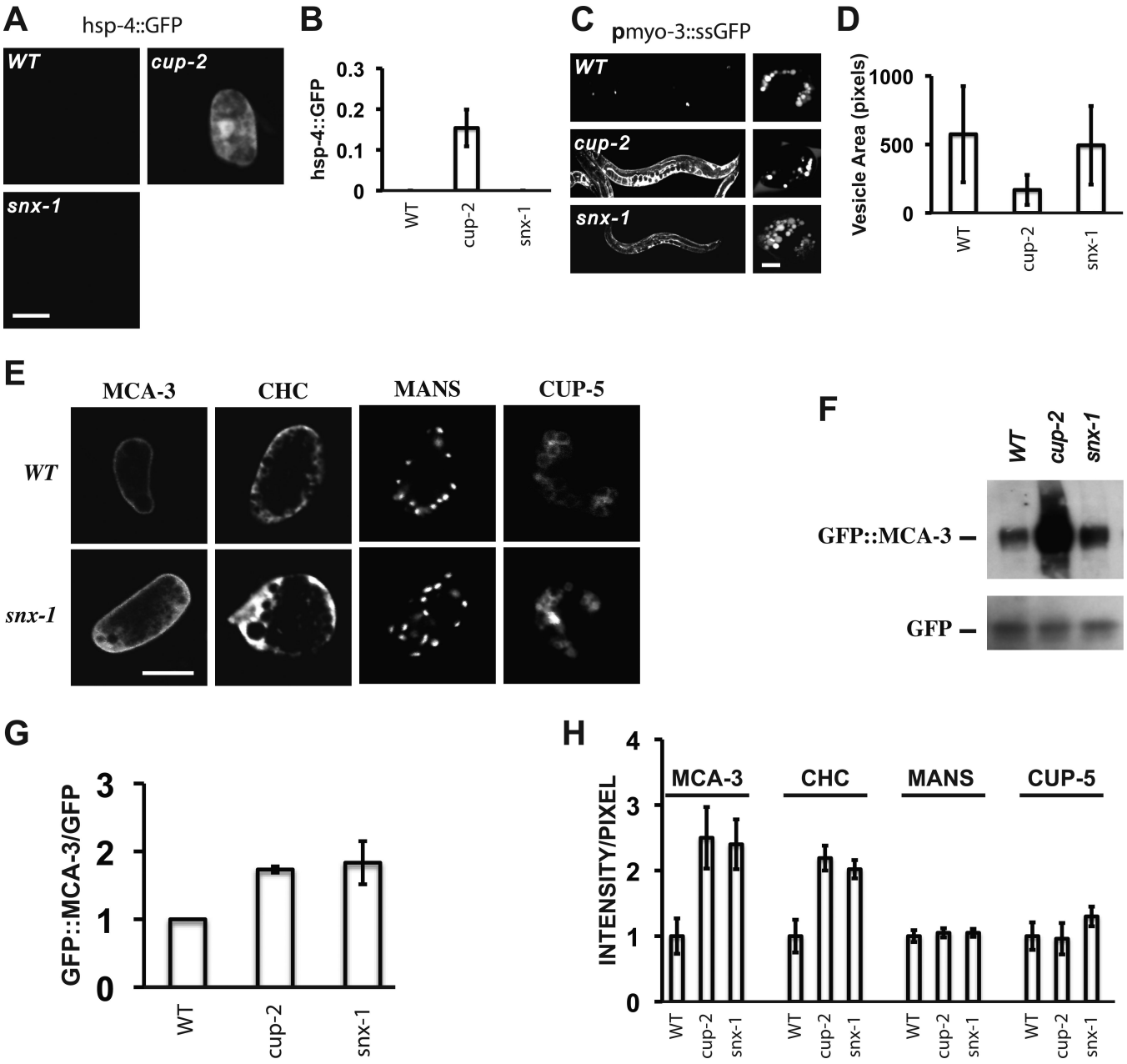

Figure 2. *snx-1* Mutant Phenotypes

A) Confocal images of coelomocytes in wild type, *cup-2(ar506)*, *snx-1(tm847)*, and double mutants adult hermaphrodites carrying the *hsp-4::GFP* transgene and grown at 20°. B) Quantitation of the average intensity per pixel of GFP in the nuclei of coelomocytes of strains from panel A. C) Confocal images of wild type, *cup-2(ar506)*, *snx-1(tm847)*, and double mutants adult hermaphrodites carrying the p*myo-3::ssGFP* transgene and grown at 20°. For each strain, the left column shows worms at a low magnification and the right column shows individual coelomocytes at a higher magnification. D) Quantitation of the sizes of the GFP-filled vesicles in coelomocytes of strains from panel C. 1 pixel is ~0.001μm^2. E) Confocal micrographs of coelomocytes in wild type (*WT*) or *snx-1(tm847)*

(*snx-1*) adult hermaphrodites grown at 20° and expressing GFP fusions to the indicated proteins. MCA-3 is Membrane Calcium ATPase; CHC is Clathrin Heavy Chain; MANS is the Golgi marker Mannosidase II; CUP-5 is a lysosomal protein. F) Western blots probed with anti-GFP antibodies of the indicated strains carrying the same GFP::MCA-3 transgene that includes DNA that expresses GFP in the pharynx of worms. The indicated bands are GFP::MCA-3 (197 kD) and GFP (27 kD). The fluorescence intensity of the pharyngeal GFP is identical in the different strains. G) Quantitation of the bands from Western in panel F. Numbers are based on three experiments and are normalized to 1 using wild type values. H) Quantitation of the markers in panel E. Numbers were normalized to 1 using wild type values for each marker. Bar is 5 μm in all images of coelomocytes.

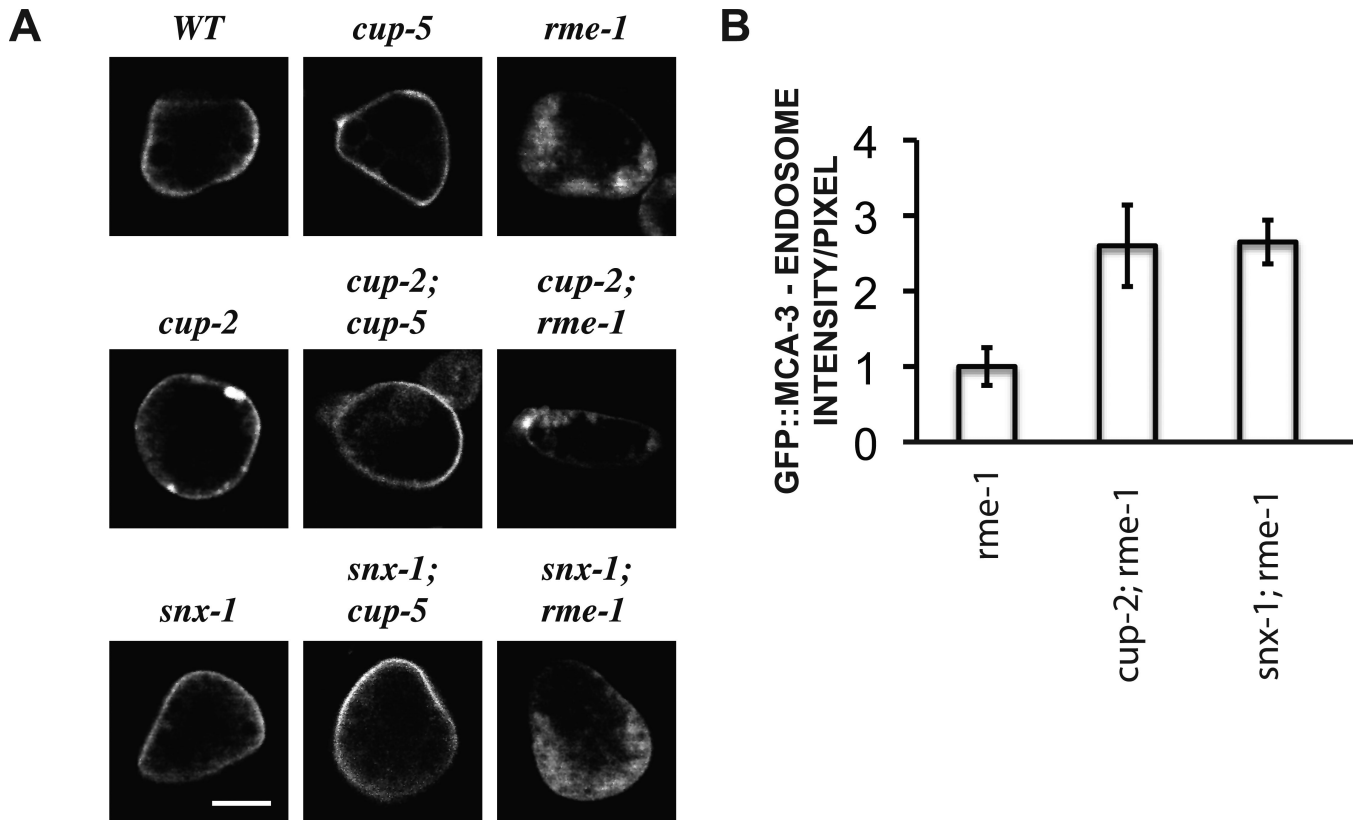

Figure 3. MCA-3 Trafficking Itinerary

A) Confocal images of coelomocytes expressing GFP::MCA-3 in the indicated strains. The images shown were not taken using the same microscopy parameters. Bar is 5 μm in all images of coelomocytes. B) Quantitation of the GFP::MCA-3 in expanded recycling endosomes of the indicated strains. Quantitation was done on images taken using the same microscopy parameters. Numbers were normalized to 1 using wild type values.

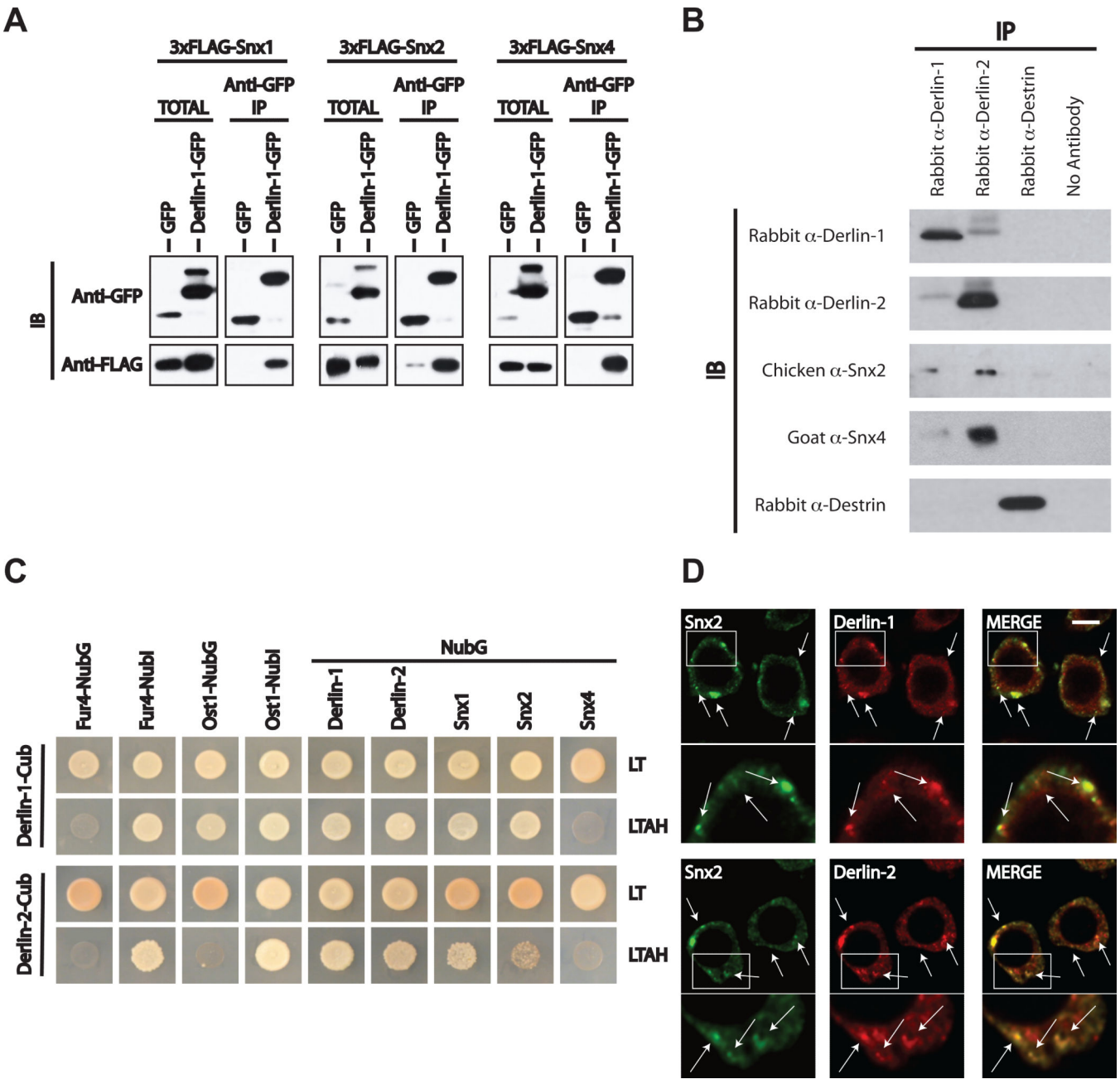

Figure 4. Mammalian Derlin and Sorting Nexin Physical Association

A) Western blots of total protein and anti-GFP IP samples after transfection of HeLa cells with plasmids that express the indicated constructs. Derlin-1, Snx1, Snx2, and Snx4 are mouse proteins. B) Western blots after immunoprecipitation of endogenous proteins using the same amounts of the indicated antibodies. Immunoprecipitation was done using the same volumes of lysates of murine RAW264.7 macrophages. C) Split-ubiquitin yeast two-hybrid assay using mouse Derlin-1-Cub and Derlin-2-Cub-expressing plasmids. The same number of yeast cells were spotted on –leu –trp (LT) plates to monitor growth without selection and on – leu –trp –ade –his + 5 mM 3-AT (LHAT) to assay physical interactions. The image is after three days of growth at 30°. D) Confocal images of RAW264.7 cells co-stained for

Derlin-1 (red) and Snx2 (green) or for Derlin-2 (red) and Snx2 (green). The bottom rows show higher magnification images of the boxed areas in the upper rows. Arrows indicate co-localization. Bar is 5 μm in lower magnification images and 0.4 μm in higher magnification images.

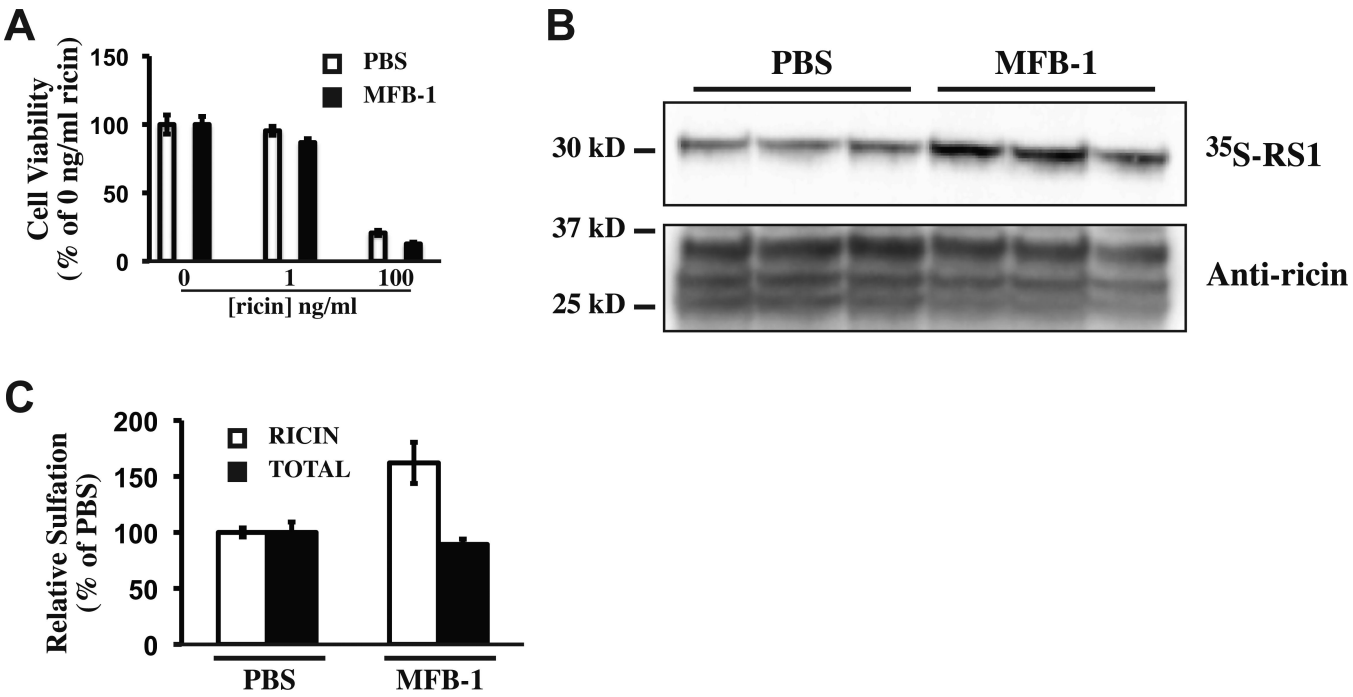

Figure 5. Ricin Retrograde Transport After Plasma Membrane Protein Misfolding

A) Viability of RAW264.7 macrophages following exposure to ricin under normal (PBS) and misfolding (MFB-1) conditions. Each assay was done in triplicate. B) Amount of sulfated RS1 (top panel) and endocytosed ricin (bottom panel) by RAW264.7 macrophages under normal (PBS) and misfolding (MFB-1) conditions. Each assay was done in triplicate. C) Quantitation of the RS1 sulfation from panel B and total sulfation of RAW264.7 macrophages under normal (PBS) and misfolding (MFB-1) conditions.

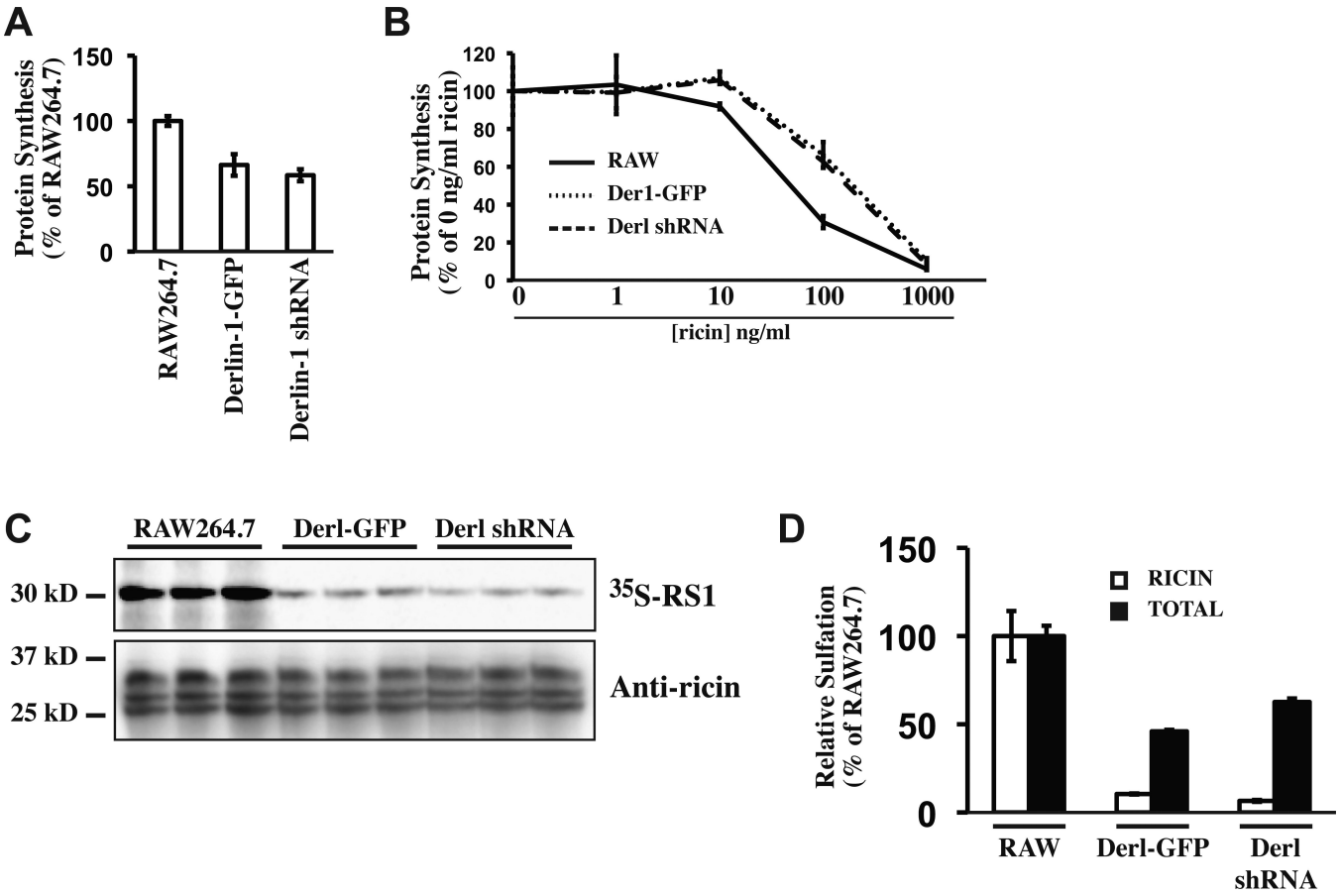

Figure 6. Derlin-1-Dependent Ricin Retrograde Transport

A) Total protein synthesis measurements in the absence of ricin using [^{3}H]leucine incorporation in RAW264.7 macrophages or RAW264.7 macrophages stably expressing the indicated constructs. Each assay was done in triplicate. B) Total protein synthesis measurements in the presence of ricin using [^{3}H]leucine incorporation in RAW264.7 (solid line), Derlin-1-GFP clone (short dashed line), and Derlin-1 shRNA clone (long dashed line). Each assay was done in triplicate. C) Amount of sulfated RS1 (top panel) and endocytosed ricin (bottom panel) in the indicated strains. Each assay was done in triplicate. D) Quantitation of the RS1 sulfation from panel C and total sulfation of the indicated strains.

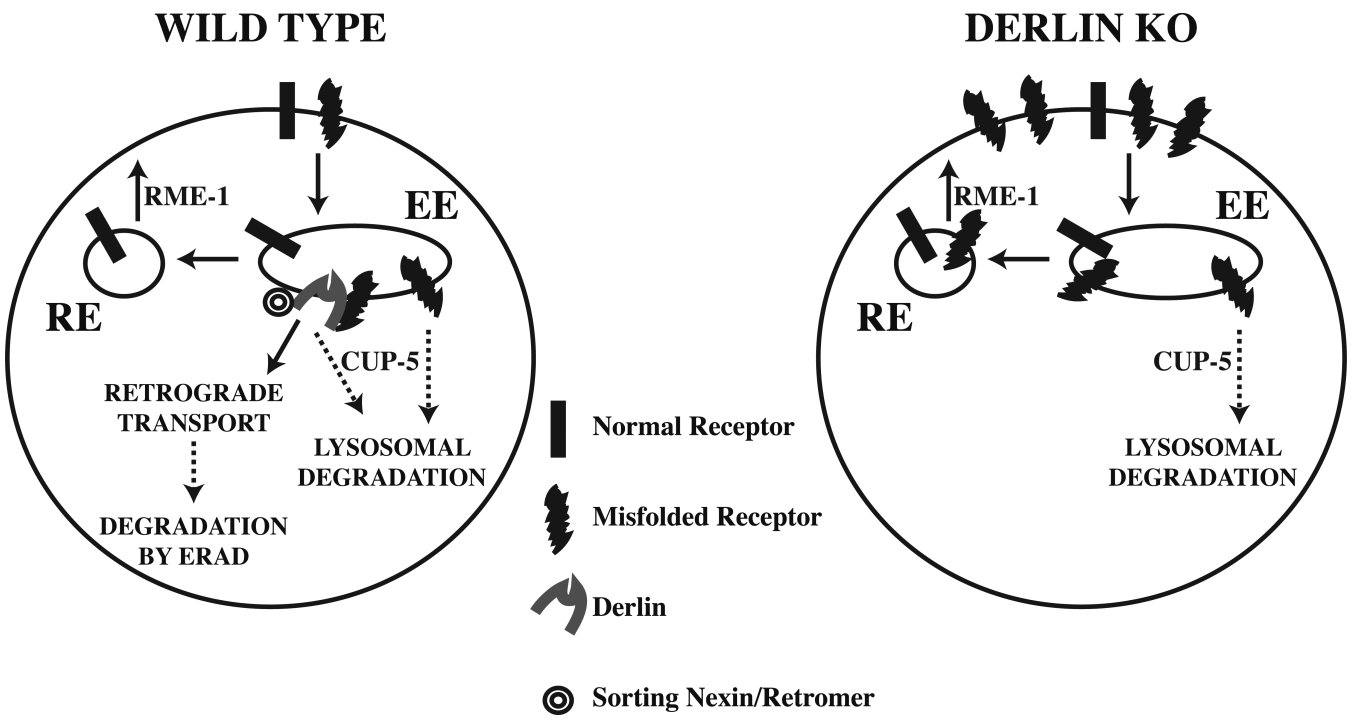

Figure 7. Model of Derlin Functions in Retrograde Transport of Misfolded Proteins

The schematic shows Derlins associating with misfolded proteins and with Sorting Nexins at the early endosome, thus targeting misfolded proteins for retrograde transport to the Golgi apparatus. Solid arrows represent trafficking itineraries that were examined in this study. Hatched arrows represent additional possible transport steps that were not examined. RME-1 regulates the recycling pathway and CUP-5 regulates lysosomal transport. EE = Early Endosome; RE = Recycling Endosome.